Ekman Layer Rectification

JAMES C. MCWILLIAMS AND EDWARD HUCKLE

Institute of Geophysics and Planetary Physics, University of California, Los Angeles, Los Angeles, California

(Manuscript received 14 January 2005, in final form 17 November 2005)

ABSTRACT

The phenomenon of oceanic Ekman layer rectification refers to how the time-mean, Ekman layer velocity profile with depth differs as a consequence of variability in the surface wind in addition to the time-mean wind. This study investigates rectification using the *K*-Profile Parameterization (KPP) model for the turbulent surface boundary layer under simple conditions of uniform density and no surface buoyancy flux or surface wave influences. The rectification magnitude is found to be significant under typical conditions. Its primary effects are to extend the depth profile deeper into the interior, reduce the mean shear, increase the effective eddy viscosity due to turbulent momentum mixing, and rotate slightly the surface velocity farther away from the mean wind direction. These effects are partly due to the increase in mean stress because of its quadratic dependence on wind speed but also are due to the nonlinearity of the turbulent mixing efficiency. The strongest influence on the rectification magnitude is the ratio of transient wind amplitude to mean wind speed. It is found that an accurate estimate of the mean current usually can be obtained by using a quasi-stationary approximation that is a weighted integral of the steady Ekman layer response over the probability density function for the wind, independent of the detailed wind history. Rectification occurs even for very high frequency wind fluctuations, though the accuracy of the quasi-steady approximation degrades in this limit (as does the validity of the KPP model). This theory is extended to include the effects of the horizontal component of the Coriolis frequency, f^y. Based on published computational turbulence solutions, a simple parameterization is proposed that amplifies the turbulent eddy diffusivity in KPP by a factor that decreases with latitude and depends on the wind orientation. The effect of $f^y \neq 0$ is to increase both the shear and the surface speed in the time-mean Ekman current for winds directed to the northeast and decrease both quantities for winds to the southwest, with weaker influences on these properties for the orthogonal directions of southeast and northwest. Furthermore, with transient winds there is significant coupling between $f^y \neq 0$ and the rectification effect; for example, the mean surface current direction, relative to the mean wind, is significantly changed for these orthogonal directions.

1. Introduction

Ekman's (1905) explanation for the structure and magnitude of near-surface currents driven by a steady wind in a uniform-density fluid is perhaps the most venerable of oceanographic theories (apart from Archimedes' hydrostatic balance). Its prediction for the depth-integrated horizontal current (i.e., the transport), namely,

$$\mathbf{T} = \hat{\mathbf{z}} \times \frac{1}{\rho_o f}\boldsymbol{\tau} \tag{1}$$

(where $\hat{\mathbf{z}}$ is the locally vertical upward unit vector, f is the vertical component of the Coriolis frequency, ρ_o is the oceanic density, and $\boldsymbol{\tau}$ is the surface tangential stress) is robustly independent of the turbulent behavior in the surface boundary layer. Its parameterization model for the turbulent momentum mixing, that the eddy vertical momentum flux acts as eddy diffusion with a constant diffusivity κ_0, is now understood to be naive (e.g., Madsen 1977). Nevertheless, the predicted current structure in this "classical" solution—a decay of speed and an anticyclonic rotation of direction descending into the interior (i.e., the Ekman spiral)—has been confirmed as qualitatively apt by various measurements (e.g., Weller 1981; Price et al. 1987; Wijffels et al. 1994; Chereskin 1995; Weller and Plueddemann 1996; Chereskin et al. 1997; Price and Sundermeyer 1999), although the predicted shape for the depth profile is not well verified.

Apart from the challenge of modeling the turbulent mixing, several other dynamical influences need to be considered for oceanic realism, including density strati-

Corresponding author address: James C. McWilliams, Dept. of Atmospheric and Oceanic Sciences, UCLA, Los Angeles, CA 90095-1567.
E-mail: jcm@atmos.ucla.edu

fication, surface buoyancy flux, surface gravity wave effects, horizontal heterogeneity (and associated upwelling), the horizontal projection of Earth's rotation vector (i.e., the horizontal Coriolis frequency, f^y), and general time variability. In this paper we focus on the latter two influences. Specifically, we ask and answer the question of how the depth profile for the low-frequency, large-scale, upper-ocean horizontal velocity, $\overline{\mathbf{u}}(z)$, is altered by the combination of high-frequency surface stress fluctuations and nonlinear turbulent vertical mixing. Then we further examine how this answer is modified by $f^y \neq 0$. If the vertical mixing had a constant eddy viscosity (as in Ekman's model), then the boundary layer model would be linear; the stress fluctuations would average out; and the average depth profile would be controlled simply by the average stress and mixing rate κ_0 and by latitude through $f(\Phi)$. The phenomenon of differences in average currents due to wind fluctuations is called boundary layer rectification. Our goals are to quantify its magnitude as a function of wind attributes and location (i.e., latitude) and to develop procedures for its inclusion in empirical analyses and models of the upper-ocean current.

In a general circulation model with complete temporal information about the surface fluxes and a boundary layer model, one can simply integrate in time and average the resulting solution in order to assess a posteriori the rectification. However, if only low-frequency fluxes are available or if velocity measurements—to be used, for example, in data assimilation—must be smoothed in time to obtain a meaningful "mean current," then some time-averaged model must be used that, in particular, includes a representation of the rectification.

This paper is a preliminary inquiry into rectification for the classically idealized circumstances of uniform density, horizontal homogeneity, and a specified wind stress at a rigid top lid—that is, the Ekman layer problem. [A germane but different study of Ekman layer rectification is Price and Sundermeyer (1999), which focuses on the influence of diurnally varying surface buoyancy flux; this is further discussed in section 6.] In section 2 the problem is posed in more detail, the *K*-Profile Parameterization (KPP) boundary layer model (Large et al. 1994) is specified, and a generalization of KPP is proposed to encompass $f^y \neq 0$. In section 3 the steady solution for the KPP model is compared with both Ekman's model and some recent computational turbulence simulations. In section 4 the rectification results using the KPP model are presented, and a quasi-stationary approximation is defined and assessed that estimates the rectification without making a detailed time integration. Section 5 reconsiders both the steady and transient solutions with $f^y \neq 0$. Section 6 contains a summary and discussion of our findings.

2. Boundary layer model

a. *Posing the problem*

In a given geographical location, we solve the following equations for the horizontal current, $\mathbf{u}(z, t) = (u, v)$, with zero horizontal pressure gradient and advection; vertical mixing as prescribed by the KPP model (Large et al. 1994); specified surface stress $\tau(t)$; a simple model for damping of inertial currents in the boundary layer (i.e., current rotations with frequency f) due to vertical radiation induced by lateral potential vorticity gradients (Pollard and Millard 1970; D'Asaro et al. 1995; van Meurs 1998); and zero momentum flux through the lower boundary at $z = -H$ (assumed to lie well below the surface boundary layer). The horizontal momentum balance is

$$\frac{\partial \mathbf{u}}{\partial t} + f\hat{\mathbf{z}} \times \mathbf{u} = \frac{\partial \mathcal{F}^{\mathbf{u}}}{\partial z} - R\mathbf{u}. \tag{2}$$

The vertical momentum flux due to turbulent mixing is represented by $\mathcal{F}^{\mathbf{u}}$, and R is the damping rate for currents due to vertical radiation of inertial waves into the oceanic interior.

The boundary condition at $z = 0$ is

$$\mathcal{F}^{\mathbf{u}}(0) = \frac{\boldsymbol{\tau}}{\rho_o} = C_D \frac{\rho_a}{\rho_o} |\mathbf{u}^a| \mathbf{u}^a \equiv u_*^2 \hat{\boldsymbol{\theta}}_*, \tag{3}$$

where C_D is the drag coefficient, ρ_o and ρ_a are the oceanic and atmospheric densities, $\mathbf{u}^a$ is the wind near the surface, u_* is the friction velocity, θ_* is the angular direction of the wind stress (with θ_* the angle of the wind from east), and $\hat{\boldsymbol{\theta}}_* = [\cos(\theta_*), \sin(\theta_*)]$ is a unit vector in that direction. The boundary condition at $z = -H$ is

$$\mathcal{F}^{\mathbf{u}}(-H) = 0. \tag{4}$$

For the boundary value problem in (2)–(4), the transport relation (1) holds if the damping term with R is neglected; for the small R value chosen in sections 3 and 4, this approximation is quite accurate. The vertical momentum flux (i.e., turbulent Reynolds stress) is formally defined by

$$\mathcal{F}^{\mathbf{u}}(z) = -\langle w\mathbf{u} \rangle, \tag{5}$$

where ω is the vertical velocity and the angle brackets denote an average over the turbulent motions. The depth profile of $\mathcal{F}^{\mathbf{u}}(z)$ is modeled by KPP in (9).

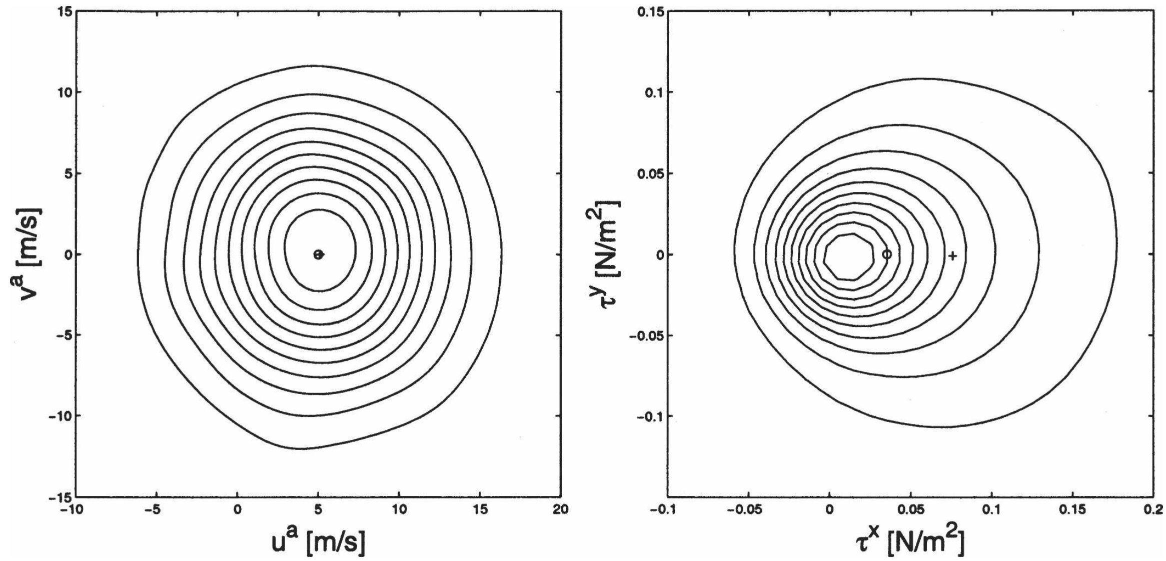

FIG. 1. Probability density functions for (left) wind and (right) wind stress for a steady wind with $\overline{u}^a = 5$ m s^{-1} plus a two-dimensional, transient, Markov wind with $\Sigma_u^a = \Sigma_v^a = |\overline{u}^a|$. In each panel + marks the mean value, and O marks the value when the transient component is absent.

b. Wind

The wind, $\mathbf{u}^a(t)$, is decomposed into its time average (denoted by overbar) and fluctuation (denoted by prime),

$$\mathbf{u}^a(t) = \overline{\mathbf{u}}^a + \mathbf{u}^{a\prime}. \tag{6}$$

There are corresponding mean and fluctuation components of τ after substituting into (3). In this theoretical study of rectification, we will assume that each of the fluctuation wind components, $\mathbf{u}^{a\prime} = (u^{a\prime}, v^{a\prime})$, is either time periodic, that is,

$$u^{a\prime} = u_0^{a\prime} \sin(\omega_0 t + c_0) \quad \text{and} \quad v^{a\prime} = u_0^{a\prime} \cos(\omega_0 t + c_0), \tag{7}$$

or is the outcome of an independent first-order Markov process for each wind component, for example, a zonal velocity whose increments over a time step dt are

$$du^{a\prime} = -\frac{dt}{T^a} u^{a\prime} + \left(\frac{2\Sigma^{a2}\, dt}{T^a}\right)^{1/2} r'. \tag{8}$$

In the Markov model, T^a is the memory time, Σ^{a2} is the variance of $u^{a\prime}$, and r' is Gaussian white noise with zero mean and unit variance. The resulting fluctuation frequency spectrum is broadband in ω, flat for $\omega < 1/T^a$, and decreasing as ω^{-2} for $\omega \gg 1/T^a$.

Figure 1 illustrates the outcome from (6) and (8) using the standard case parameters defined in section 4. (Since the time history is not shown here, there is no evident dependence on T^a.) The probability density function (PDF) for the wind is symmetric about its mean value, but the PDF for the stress is skewed toward larger stresses in the direction of the mean wind. Furthermore, the mean stress is much larger than the stress for $\overline{u}^a$ alone because of the quadratic dependence in (3). This indicates one of the two primary rectification mechanisms: transient winds increase the mean stress, and this occurs no matter what the time scale of the fluctuation.

c. KPP for the Ekman layer

In the situation with uniform density and a surface stress, the KPP rules for the Reynolds stress in the surface boundary layer are the following:

$$\mathcal{F}^{\mathbf{u}}(z) = \kappa(z)\frac{\partial \mathbf{u}}{\partial z},$$

$$\kappa(z) = c_1 u_* h G(\sigma), \quad \sigma = -\frac{z}{h},$$

$$h = c_2 \frac{u_*}{f}, \quad \text{and}$$

$$G(\sigma) = \sigma(1-\sigma)^2 + H(\sigma_o - \sigma)\frac{(\sigma - \sigma_o)^2}{2\sigma_o}, \tag{9}$$

where u_* is defined in (3), h is the boundary layer depth, $c_1 = 0.4$ (i.e., von Kármán's constant), $c_2 = 0.7$, $\sigma_o = 0.05$, and $H(p)$ is the Heaviside step function (equal to 1 for $p > 0$ and 0 for $p < 0$). The normalized depth σ increases from 0 at the surface to 1 at the bottom of the boundary layer. The second term in G has not been used previously in KPP. It is nontrivial only very near the surface and has the effect of locally regularizing the logarithmic singularity in $\mathbf{u}(z)$ as $z \rightarrow 0$ associated with the classical surface layer depth profile for a wall-bounded shear flow. Its physical justification is additional mixing in the oceanic boundary layer due to surface gravity wave breaking and mixing within a shallow layer of thickness $\sigma_o h$ [cf. the scaling of this layer thickness with the wave height in Terray et al. (1996)]. In the context of this paper, it has no significant influence on the rectification results, so our other reasons for including it are mathematical aesthetics and computational regularity.

It is customary in oceanic models to increment the boundary layer eddy viscosity with a background eddy viscosity that extends vertically into the interior. We follow this practice here with a vertically constant viscosity, $\kappa_b = 10^{-4}\ \mathrm{m^2\,s^{-1}}$, whose value is much smaller than the peak boundary layer values in (9). Beyond modestly improving the smoothness of the solutions, it plays no significant role and will be ignored for the rest of the paper.

d. Horizontal Coriolis frequency

Earth's rotation vector $\boldsymbol{\Omega}_e$ is upward through the North Pole at a rate of 1 cycle per day. In a local Cartesian coordinate system (x, y, z)—with z outward against gravity and its origin at Earth's surface, x eastward, and y northward—the rotation vector is decomposable as

$$\boldsymbol{\Omega}_e = \frac{1}{2}(f\hat{\mathbf{z}} + f^y\hat{\mathbf{y}}), \tag{10}$$

with

$$f = 2|\boldsymbol{\Omega}_e|\sin(\Phi), \quad f^y = 2|\boldsymbol{\Omega}_e|\cos(\Phi), \tag{11}$$

and the associated Coriolis force,

$$-2\boldsymbol{\Omega}_e \times \mathbf{u} = (fv - f^y w)\hat{\mathbf{x}} + (-fu)\hat{\mathbf{y}} + (f^y u)\hat{\mathbf{z}}. \tag{12}$$

Latitude is $\Phi \in [-\pi/2, \pi/2]$, and f has different signs in the two hemispheres, but $f^y \geq 0$ everywhere.

In the preceding discussion of the boundary layer model, f^y has been ignored, as it usually is for planetary boundary layer studies, even though $f^y = 0$ only at Earth's Poles ($\Phi = \pm\pi/2$). However, both Coleman et al. (1990) and Zikanov et al. (2003) solved computational problems for the turbulent Ekman layer (more fully described in section 3) with $f^y \neq 0$. Their results[1] indicate that f^y has a significant effect mainly through a dependence on the wind stress direction, θ: for $\theta = \theta_0 \approx \pi/4$, the turbulent intensity and vertical Reynolds stress are greatly diminished relative to $f^y = 0$, and for $\theta = \theta_0 + \pi \approx 5\pi/4$ they are greatly enhanced. The effect decreases with latitude and vanishes at the Poles, and in the Southern Hemisphere the wind direction for minimum turbulent intensity and Reynolds stress is $\theta_0 \approx -\pi/4$ [since the transformation, $(f, y', v', \theta) \rightarrow (-f, -y', -v', -\theta)$, leaves the problem unchanged in a horizontally rotated coordinate system with the x' axis aligned with the surface stress]. The mechanism for this effect, first discussed in Garwood et al. (1985a,b) is a systematic transfer between vertical and horizontal turbulent velocity fluctuation variances that depends on the orientation of the wind stress relative to $f^y\hat{\mathbf{y}}$. In particular, for $f, f^y > 0$, $\theta = \theta_0 + \pi = 5\pi/4$ favors an Ekman surface current with $u < 0$ that accelerates $\omega < 0$ by (12) and positively reinforces the Coriolis force in the zonal momentum equation where $v > 0$.

In a mean-field boundary layer model with parameterized turbulent fluxes, like (2), the horizontal component of the Coriolis frequency does not appear explicitly since the mean w is zero and the horizontal component $\propto f^y$ vanishes in the Coriolis force (12). However, the effects of $f^y \neq 0$ may be included in the parameterized fluxes, $\mathcal{F}^{\mathbf{u}}(z)$, through a modified form of KPP. Although the present collection of computational turbulent Ekman layer solutions with $f^y \neq 0$ does not allow a precise determination of how the KPP model should be modified, the diagnosed depth profile for eddy viscosity (Zikanov et al. 2003, their Fig. 8c) shows an approximate dependence on wind direction and latitude that simply multiplies the $\kappa(z)$ for $f^y = 0$ in (9) by a depth-independent factor, $J(\theta, \Phi)$, when $f^y \neq 0$. An approximate fit to this amplification factor can be made using the following functional form for J:

$$J(\theta, \Phi) = 1 + \frac{A^2}{2(1 - A)} - A\left(\frac{1 - A/2}{1 - A}\right)\cos(\theta - \theta_0),$$

where

$$A(\Phi) = A_0\cos(\Phi). \tag{13}$$

This function has no fundamental justification, but it is both relatively simple and has the following desirable

[1] This interpretation of Zikanov et al. (2003) requires that we interpret their γ as the angle from the wind stress direction to the north direction measured in a counterclockwise rotational sense. This contradicts their Fig. 1 sketch and their textual description of the angle of minimum response, but it is consistent with the system of equations solved [their (2.1)–(2.4)].

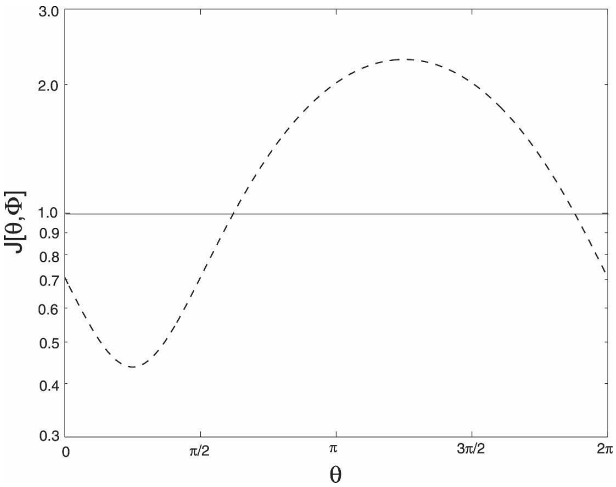

FIG. 2. Diffusivity amplification factor, $J(\theta, \Phi)$ from (13), plotted on a semilogarithmic scale for $\Phi = \pi/6$, $A_0 = 0.65$, and $\theta_0 = \pi/4$.

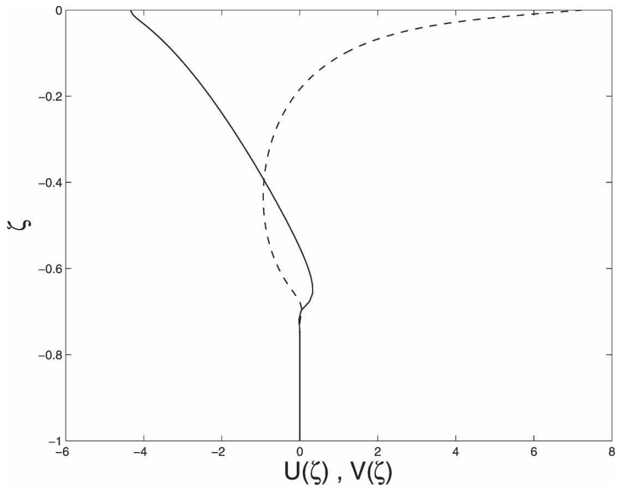

FIG. 3. Nondimensional mean zonal and meridional velocity profiles, $U(\zeta)$ (dashed line) and $V(\zeta)$ (solid line), for a steady-state Ekman layer with a steady zonal wind using the KPP model with $\tilde{R} = 0.023$.

properties that match the available evidence about the effects of $f^y \neq 0$:

- $0 < J < \infty$ if $0 < A_0 < 1$.
- $J = 1$ when $\Phi = \pm\pi/2$ since $A(\pm\pi/2) = 0$, and J is most different from 1 when $\Phi = 0$.
- J is monotonic in Φ for a fixed θ, and J is monotonic in θ between θ_0 and $\theta_0 \pm \pi$ for a fixed Φ.
- J is smallest, $1 - A_0$, when $(\theta, \Phi) = (\theta_0, 0)$ and is largest, $1/(1 - A_0)$, when $(\theta, \Phi) = (\theta_0 \pm \pi, 0)$.
- The amplification or reduction of κ is geometrically symmetric in θ; that is, if $J(\theta_0, \Phi_*) = 1 - A_* \leq 1$ for a given $\Phi = \Phi_*$, then the smallest modified diffusivity is $(1 - A_*)\kappa$ at $\theta = \theta_0$ and the largest is $\kappa/(1 - A_*)$ at $\theta = \theta_0 \pm \pi$.

To approximately fit the evidence presented in Zikanov et al. (2003, their Fig. 8c), we choose

$$A_0 = 0.65 \quad \text{and} \quad \theta_0 = \frac{\pi}{4}. \tag{14}$$

The amplification factor is plotted in Fig. 2. With the particular functional form (13), the interval in θ where $J > 1$ is somewhat larger than the interval where $J < 1$. Given the presently limited basis for choosing J, the aptness of this feature cannot be assessed.

3. Steady wind results

a. Nondimensionalization and KPP solution

A steady solution to (2) has no acceleration term. It can be transformed to the following nondimensional boundary value problem:

$$\hat{\mathbf{z}} \times \mathbf{U} = \frac{\partial}{\partial \zeta}\left[K(\zeta)\frac{\partial \mathbf{U}}{\partial \zeta}\right] - \tilde{R}\mathbf{U},$$

$$K\frac{\partial \mathbf{U}}{\partial \zeta}(0) = \hat{\mathbf{x}}, \quad \text{and} \quad U(-\tilde{h}) = 0, \tag{15}$$

where $\hat{\mathbf{x}}$ is the unit vector in the east direction. The transformation is based on a rescaling of variables by u_* and f and a rotation by the angle $-\theta_*$. The transformed quantities are defined by

$$\zeta = \frac{f}{u_*}z, \quad \tilde{h} = \frac{f}{u_*}h = c_2,$$

$$\mathbf{U} = u_*^{-1}\mathrm{ROT}_{-\theta_*}(\mathbf{u}),$$

$$K = \frac{f}{u_*^2}\kappa = c_1c_2G\left(\frac{\zeta}{\tilde{h}}\right), \quad \text{and} \quad \tilde{R} = \frac{1}{f}R. \tag{16}$$

The rotation operator by an angle ϕ is defined by

$$\mathbf{A} \equiv \mathrm{ROT}_\phi(\mathbf{a}) \equiv [a\cos(\phi) - b\sin(\phi), a\sin(\phi) + b\cos(\phi)] \tag{17}$$

when applied to the horizontal vector, $\mathbf{a} = (a, b)$. (We set $J = 1$ here and in the next section, deferring the effects of $f^y \neq 0$ until section 5.) Thus, the dependences on wind stress and Coriolis frequency are explicitly contained in (16): the Ekman currents vary in magnitude linearly with u_* and rotate with θ_*; the current depth scale varies with u_*/f, and the transport $\mathbf{T}$ varies with u_*^2/f.

The solution to (15) for $\tilde{R} = 0.023$ (section 4) is plotted in Fig. 3, and the associated eddy viscosity profile,

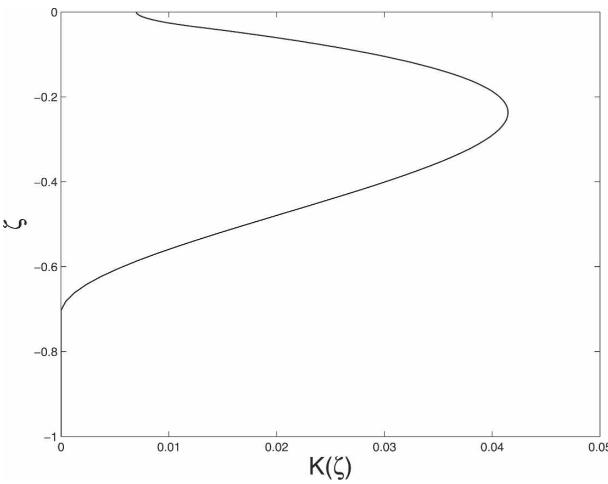

FIG. 4. Nondimensional eddy viscosity profile $K(\zeta)$ for a steady-state Ekman layer using the KPP model.

$K(\zeta)$, is plotted in Fig. 4. The surface current is oriented with an angle of $\beta = 31°$ to the right of the wind (in the Northern Hemisphere), and the current speed decays with depth and its direction rotates farther to the right. The eddy viscosity peaks at a depth of $\zeta = -0.23$ with a magnitude of $K = 0.41$.

b. Comparison with other steady solutions

We can compare the KPP solution of (15) with the classical solution for constant K. The depth-integrated square difference in $\mathbf{U}(\zeta)$ in Fig. 3 is minimized with the diffusivity value, $K_0 = 0.27$. The classical solution has a weaker surface current, $\mathbf{U}(0)$, that is rotated by a greater amount ($\beta = 45°$) to the right of the stress (Fig. 5). The classical $\mathbf{U}(\zeta)$ has weaker shear both near the surface and near its interior edge because its K value is larger there than KPP's. At the interior edge the classical solution extends farther in depth, for the same reason. Associated with the layer-edge shear differences, the classical Ekman spiral has a fatter bow shape than KPP's. As required by the boundary conditions, the solutions have the same transport, $\mathbf{T}$ (neglecting the effect of $\tilde{R}$).

How accurate is the KPP model for the Ekman layer problem? The best available answers come from laboratory experiments and computational turbulence solutions. Coleman et al. (1990) and Coleman (1999) present direct numerical simulations (DNS) of the rotating Navier–Stokes equations for the problem of a steady interior flow above a solid (i.e., no slip) boundary at several different Reynolds numbers up to 10^3. This solid-boundary atmospheric problem can be approximately transformed into the oceanic problem by inverting the vertical coordinate, equating the surface stress direction and magnitude (i.e., $|\tau| = \rho_a u_*^{a2} = \rho_o u_*^{o2}$), and transforming the velocity by the formula

$$\mathbf{u}^o\left(z^o = -\frac{u_*^o}{u_*^a} z^a\right) = \frac{u_*^o}{u_*^a}[\mathbf{u}^a(z^a = \infty) - \mathbf{u}^a(z^a)]. \tag{18}$$

This transformation is not based on an exact equivalence because the atmospheric solution has fluctuations in τ that are absent in the oceanic steady-stress problem, and the oceanic solution has fluctuations in the surface velocity that are absent in the atmospheric velocity as $z^a \to \infty$. Nevertheless, there is good qualitative agreement with the KPP solution (Fig. 5), except very

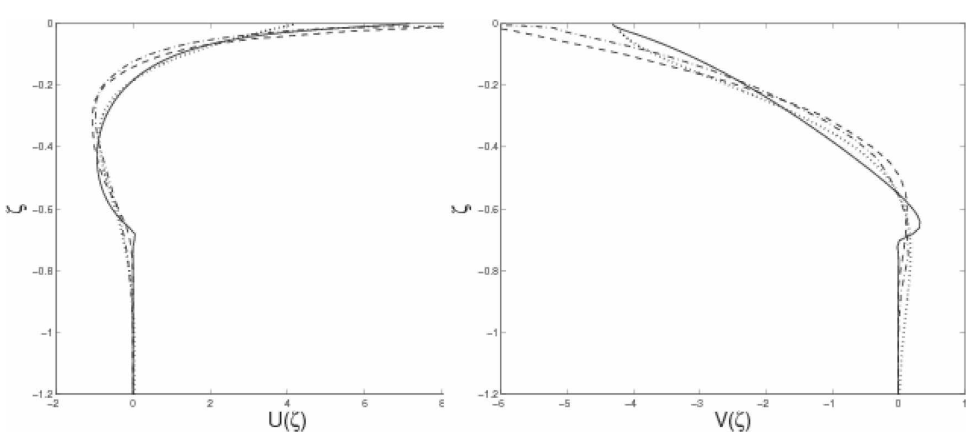

FIG. 5. Nondimensional mean velocity profiles $\mathbf{U}(\zeta)$ for an Ekman layer with a steady zonal wind: KPP with $\tilde{R} = 0.023$ (solid line), Zikanov et al. (2003) (dashed line), Coleman (1999) (dash–dotted line), and constant-K (=0.027) optimally fit to the KPP solution (dotted line). The respective values for surface angle, β, are 31°, 33°, 19°, and 45°.

near the surface, where a viscous sublayer, associated with the no-slip boundary condition and the consequent absence of velocity fluctuations, exhibits very large shear. The surface current rotation angle is $\beta = 19°$ in Coleman (1999), although it is larger in the Coleman et al. (1990) solutions and in the laboratory experiments of Caldwell et al. (1972) (both at lower Reynolds numbers and with the unoceanic surface boundary condition), hence closer to the KPP value $\approx 30°$. The diagnosed eddy diffusivity—minus the ratio of Reynolds stress and mean shear—also has a convex shape (cf. Fig. 15 of Coleman et al. 1990), and the bow in the Ekman spiral is again thinner than in the classical solution.

Zikanov et al. (2003) presents a large-eddy simulation (LES) for the oceanic problem with constant surface stress, using a "dynamic" subgrid-scale parameterization (Germano et al. 1991). It shows similar qualitative agreements in its differences from the classical Ekman solution (Fig. 5) and in the convex shape for $K(\zeta)$, albeit with a somewhat smaller peak magnitude than in Fig. 4 (cf. Fig. 5 of Zikanov et al. 2003). The surface angle value ($\beta = 33°$) is close to the KPP solution's value. This LES solution is clearly distinguished from the classical solution in its smaller surface angle, increased surface velocity, and diminished depth extent. The largest discrepancies among the different solutions occur in the surface speed, $|\overline{\mathbf{U}}(0)|$, which is closely related to the discrepancies in near-surface shear. This is a notoriously sensitive flow property in boundary layer simulations; e.g., different LES models with different subgrid-scale parameterizations differ in the near-surface shear magnitude by a factor of 2 (N.B., Fig. 4 of Andren et al. 1994). (The near-surface region is also where the Ekman problem as posed here is least realistic because of the neglect of surface wave effects.)

In summary, given the uncertainties in Reynolds number dependence and subgrid-scale parameterizations, no precise assessment standard exists for the KPP model. However, the available standards indicate that it is a reasonably accurate model with the right dependences on u_* and f, so we believe it can be used to provide credible answers for the problem of Ekman layer rectification. As we show in sections 4 and 5, the rectification and $f^y \neq 0$ effects on $\overline{\mathbf{u}}(z)$ are far larger than the disagreements seen in Fig. 5.

4. Transient wind results

a. Standard parameters

To investigate rectification, we define a standard case and choose to show the results dimensionally (N.B., the overall u_* and f dependences in section 3). The mean wind is $\overline{u}^a = 5$ m s^{-1} with $\overline{v}^a = 0$ (N.B., when $f^y = 0$ the solution is rotationally symmetric with respect to direction). The transient wind is from an independent Markov process (8) for each direction. In the standard case, $\Sigma_u^a = \Sigma_v^a = 5$ m s^{-1} (i.e., $= |\overline{u}^a|$), and $T^a = 0.86 \times 10^5$ s (1 day). We choose a latitude of $\Phi = 30°$N ($f = 0.73 \times 10^{-4}$ s^{-1}), and the inertial-propagation decay time is 7 days ($R = 1.7 \times 10^{-6}$ s^{-1}, $\tilde{R} = 0.023$). The vertical domain depth is $H = 300$ m, and we restrict our attention to cases in which $h(t) < H$ for all times in the integration.

b. Quasi-stationary approximation

For a statistically stationary, time-varying wind $\mathbf{u}^a(t)$, we can calculate the time-mean Ekman current $\overline{\mathbf{u}}(z)$ by integrating (2) in time and averaging the resulting current $\mathbf{u}(z, t)$. Alternatively, we can make the quasi-stationary approximation that assumes that the instantaneous current is close to its stationary response to the instantaneous winds for the purpose of calculating the time average. With this assumption the mean current can be equivalently calculated as a weighted integral based on the single-time PDF for the wind, which we express in terms of its stress attributes $P(u_*, \theta_*)$. The probability integral is defined by

$$\overline{\mathbf{u}}_{QS}(z) = \int_0^\infty u_*\, du_* \int_{-\pi}^{\pi} d\theta_*\, P(u_*, \theta_*) u_* \mathrm{ROT}_{\theta*} \times \left[\mathbf{U}\left(\frac{u_*\zeta}{f}\right) \right], \tag{19}$$

subject to the usual normalization condition for a PDF,

$$\int_0^\infty u_*\, du_* \int_{-\pi}^{\pi} d\theta_*\, P(u_*, \theta_*) = 1. \tag{20}$$

Alternatively, we could express these PDF integrals in terms of (u^a, v^a) rather than (u_*, θ_*) since there is a unique transformation between them by (3).

c. Effective eddy diffusivity

To interpret the mean turbulent mixing due to rectification, we define an effective eddy viscosity $\kappa_*(z)$ such that (2) is satisfied for the mean-velocity depth profile $\overline{\mathbf{u}}(z)$, with no tendency term and with an effective eddy viscosity expression for $\mathcal{F}^{\mathbf{u}} = \kappa_* \partial\overline{\mathbf{u}}/\partial z$. Since a scalar κ_* will not generally satisfy the vector momentum equation, we determine the former from a vector dot product of momentum with the vector mean shear. Assuming vanishing κ_* as $z \to -\infty$, the resulting formula is

$$\kappa_*(z) = \left\{\frac{\partial \overline{u}}{\partial z}\left[\int_{-\infty}^{z}(-f\overline{v} + R\overline{u})\,dz\right] + \frac{\partial \overline{v}}{\partial z}\left[\int_{-\infty}^{z}(f\overline{u} + R\overline{v})\,dz\right]\right\}\Bigg/\left[\left(\frac{\partial \overline{u}}{\partial z}\right)^2 + \left(\frac{\partial \overline{v}}{\partial z}\right)^2\right]. \tag{21}$$

d. Solution measures

To estimate the magnitude of several solution properties, we define the following relative measures integrated over the full depth range: for the degree of rectification,

$$\mathrm{RECT} = \sqrt{\int dz\,\{\overline{\mathbf{u}}[z;\mathbf{u}^a(t)] - \overline{\mathbf{u}}(z;\overline{\mathbf{u}}^a)\}^2 \Big/ \int dz\,[\overline{\mathbf{u}}(z;\overline{\mathbf{u}}^a)]^2}; \tag{22}$$

for the accuracy of the quasi-steady approximation,

$$\mathrm{QSA} = \sqrt{\int dz\,[\overline{\mathbf{u}}(z) - \overline{\mathbf{u}}_{\mathrm{QS}}(z)]^2 \Big/ \int dz\,[\overline{\mathbf{u}}(z)]^2}; \tag{23}$$

and for the magnitude of the fluctuating currents,

$$\mathrm{FLUC} = \sqrt{\int dz\,\overline{[\mathbf{u}(z,t) - \overline{\mathbf{u}}(z)]^2} \Big/ \int dz\,[\overline{\mathbf{u}}(z)]^2}. \tag{24}$$

In each of these expressions, $\mathbf{u}(z, t)$ is the solution obtained with the KPP model.

e. Elemental rectification

The essential rectification behavior can be explained quite simply using a mixed layer model. Its aptness is justified a posteriori in the next section: although its vertical structure is inaccurate, its scaling dependences on u_* and f are the same as in the KPP model.

We assume that the current is uniform over a depth $h = cu_*/f$ and that the transport is $T = u_*^2/f$ as in (1). This implies that the current speed is $T/h = u_*/c$. We further assume that the quasi-stationary approximation holds as the wind varies. We compare the steady current for a steady wind (with friction velocity u_{*o}) with the mean current for a situation in which the wind is 2 times as strong for one-half of the time and zero for the other one-half (N.B., it has the same mean value). The difference in these two currents is the rectification effect. In the former case the speed is u_{*o}/c over a depth cu_{*o}/f, and in the latter case the speed is the same but the depth is $2cu_{*o}/f$—2 times as deep. The rectified transport is 2 times as large as for the steady wind. The solution measures above have the values RECT = 1, FLUC = 1, and QSA = 0 (by assertion).

Part of this rectification is due to the 2-times-as-large mean stress in the transient case. However, even if we take this into account in an alternative steady wind case with friction velocity $\sqrt{2}u_{*o}$, its mean stress and transport are the same as in the transient case, but its mean current—with speed $\sqrt{2}u_{*o}/c$ over a depth $cu_{*o}/\sqrt{2}f$—is faster and shallower (but faster and deeper than with the original steady wind). In this alternative case, RECT = 0.54 is still sizable.

f. Rectification in the KPP model

The mean currents and effective diffusivities for the standard transient wind case, its companion steady wind case, and an alternative steady wind case with the same mean stress (i.e., the + value in Fig. 1, right) are shown in Figs. 6 and 7. The mutual relations among the mean currents and transports here are qualitatively similar to the elemental rectification example above.

The rectified current extends much deeper into the ocean compared to the steady wind current, although the speeds are similar. Here RECT = 0.67. The quasi-stationary approximation (19) is quite accurate (QSA = 0.04), even though the fluctuations are large (FLUC = 3.2) and the Markov wind memory time is not particularly long (T^a = 1 day). The angle β of the rectified surface current[2] is 32° to the right of the mean stress, which is only modestly larger than the steady wind angle of 31°. The effective diffusivity $\kappa_*(z)$ both reaches much deeper and is much larger, by nearly a factor of 5. For this standard transient case, $\kappa_*(z)$ is also about 2 times as large as $\overline{\kappa}(z)$ (not shown), and their depth profiles are similar.

The alternative steady case with the same mean stress has currents that penetrate to a depth intermediate between the other two currents, but its surface speed is larger than either of the other two (Fig. 6). Its transport is the same as the rectified transport [since τ fluctuations average out in (1)], and its surface rotation angle is the same steady value of 31°. Its diffusivity profile $\kappa_*(z)$ is also intermediate between the other two cases' profiles (Fig. 7). Thus, the rectification effect amplifies the penetration depth and mixing efficiency even beyond what can be associated with the increased mean stress in (16).

[2] β is a highly variable quantity for finite-time averages with transient wind forcing. The statistical results quoted here are accurate to a fraction of a degree, which requires about 100 yr of integration to achieve.

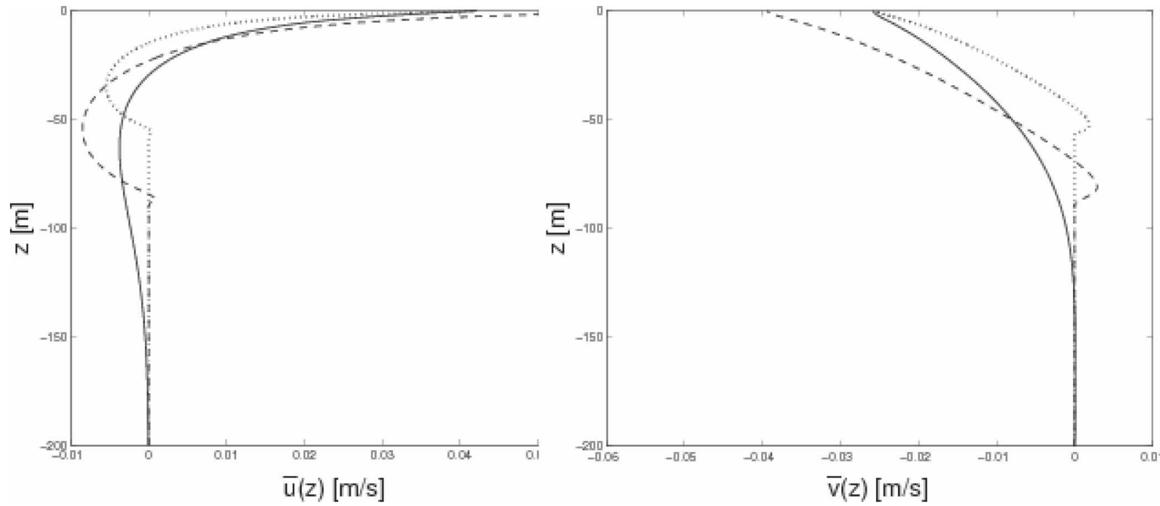

FIG. 6. Dimensional mean velocity depth profiles $\overline{\mathbf{u}}(z)$ (m s^{-1}) using the KPP model for a steady wind with $\overline{u}^a = 5$ m s^{-1} (dotted line), an additional two-dimensional, transient wind with $\Sigma_u^a = \Sigma_v^a = |\overline{u}^a|$ and $T^a = 1$ day (solid line), and a different steady wind to the east with the same mean stress as in that shown with the solid line (dashed line), for (left) $\overline{u}(z)$ (m s^{-1}) and (right) $\overline{v}(z)$.

Another feature of these solutions is the Ekman spiral, namely, the rotation of the direction of the horizontal mean current with depth (Fig. 8). As expected from the preceding plots, the surface angle (i.e., β) is nearly the same for the different cases, but the spiral is a more rapidly varying function of depth for steady winds than it is with rectification effects, even when the change in mean stress (here the expansion of the vertical scale) is taken into account. Note the rapid variation of angle especially near the surface. Ralph and Niiler (1999) and Niiler et al. (2003) estimate the mean angle of the ageostrophic current at 15-m depth relative to the surface wind and stress, over different ensembles of drogued drifting buoy displacements (and implicitly, wind ensembles), as 50° and 55°, respectively. This angle is a delicate quantity to estimate since it pertains to a depth both with high shear and a rapid spiraling rate and with large angle variations as the depth scale of the velocity profile varies with the wind forcing. Nevertheless, the 15-m angle in these solutions is markedly greater than the empirical estimates. While there may be buoyancy and stratification influences (section 6), it seems likely that this discrepancy is mostly due to the absence here of the combined surface wave effects of breaking and wave-averaged vortex force, which act

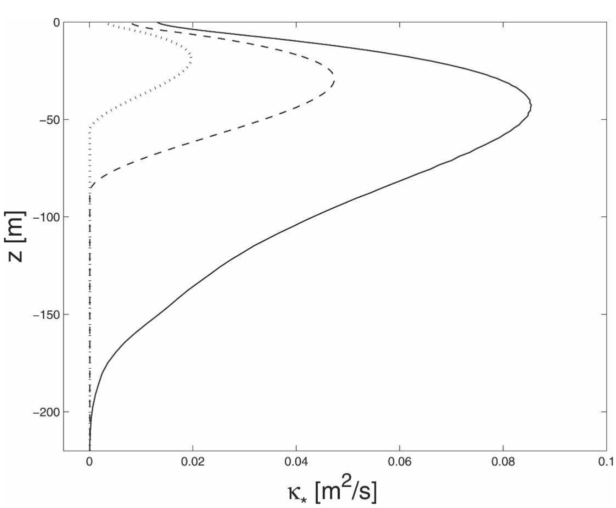

FIG. 7. Dimensional effective viscosity depth profiles $\kappa_*(z)$ (m^2 s^{-1}) for the same cases as in Fig. 6.

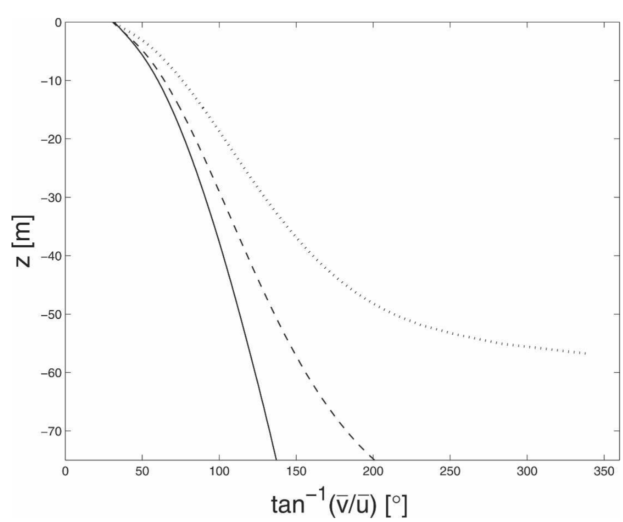

FIG. 8. Vertical profiles of the angle of the mean horizontal current relative to the mean surface stress direction for the same cases as in Figs. 6 and 7. At $z = 0$ this angle is the same as β.

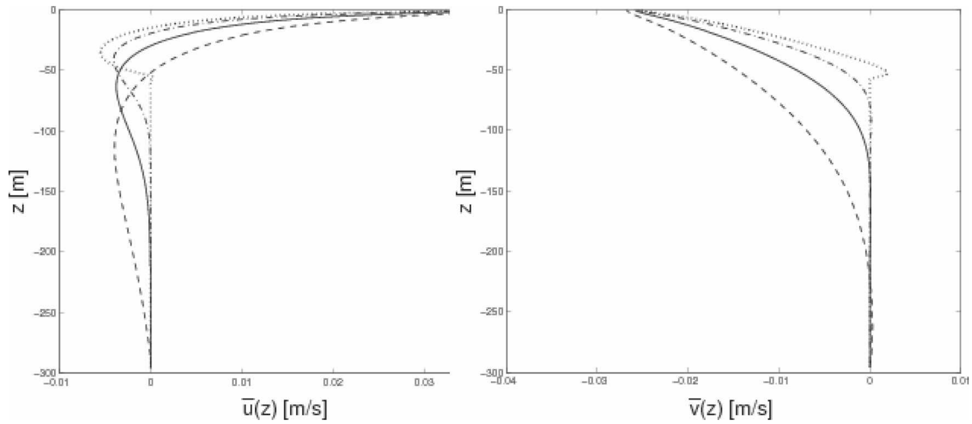

FIG. 9. Dimensional mean velocity profiles $\overline{\mathbf{u}}(z)$, using the KPP model for a steady wind with $\overline{u}^a = 5$ m s^{-1} and an additional two-dimensional, transient wind with $\Sigma_u^a = \Sigma_v^a$ equal to 0 (dotted line), $0.5|\overline{u}^a|$ (dash–dotted line), $1.0|\overline{u}^a|$ (solid line), and $2.0|\overline{u}^a|$ (dashed line).

strongly to diminish near-surface shear (McWilliams et al. 1997; Sullivan et al. 2004). This issue will not be pursued further here.

Rectification depends on the properties of the transient wind. The most important property is its fluctuation strength: Figs. 9 and 10 show systematic dependences for both the mean current's penetration depth and effective diffusivity. RECT scales very close to linearly with Σ^a, as do FLUCT and QSA (not shown). The rotation angle of the surface current also increases linearly but weakly with Σ^a (e.g., reaching a value of 34° when $\Sigma_u^a = \Sigma_v^a = 2|\overline{u}^a|$).

The shape of $P(u_*, \theta_*)$ has an influence as well. In two alternative cases, in which either $v^{a\prime}$ or $u^{a\prime}$ is set to zero while keeping the nonzero component's variance the same as in the standard case, the mean currents with wind fluctuations only in the direction of the mean wind have nearly the same rectification (i.e., RECT = 0.57 for $\Sigma_u^a = |\overline{u}^a|$ and $\Sigma_v^a = 0$), while the mean currents with only transverse wind fluctuations have a much weaker effect (RECT = 0.28 for $\Sigma_v^a = |\overline{u}^a|$ and $\Sigma_u^a = 0$). Fluctuations in the direction of the mean wind are more effective at changing the stress magnitude—hence the vertical momentum mixing and the resulting current profile—than are fluctuations perpendicular to the mean wind. The latter change the stress direction but do so symmetrically about the mean direction using (8) and thus have no net directional effect.

The frequency content of the wind is a less important influence on the rectification magnitude. RECT varies by only about 10% when T^a varies from 0.03 to 8 days (holding Σ^a constant), but the rotation angle of the mean surface current does decrease weakly with T^a (varying approximately linearly from 36° for small T^a to 32° for $T^a = 8$ days). (Note that the quasi-stationary approximation implies that there is no rectification dependence on the frequency content of the wind.) On the other hand, FLUC varies considerably with T^a, being largest when $T^a f = O(1)$ because of the potential for an inertially resonant response in (2) (Fig. 11, right). The accuracy of the quasi-stationary approximation, not surprisingly, degrades as T^a decreases (Fig. 11, left), although QSA is still moderately small, ≈0.2, even for T^a of less than 1 h.

An alternative view of the frequency dependence of rectification is provided by using a periodic transient wind (7) with frequency ω_0 and component amplitude $u_0^{a\prime} = \sqrt{2}\overline{u}^a$ (i.e., the variance is the same as in the standard case with Markov wind), even though this is less realistic than broadband fluctuations. In general,

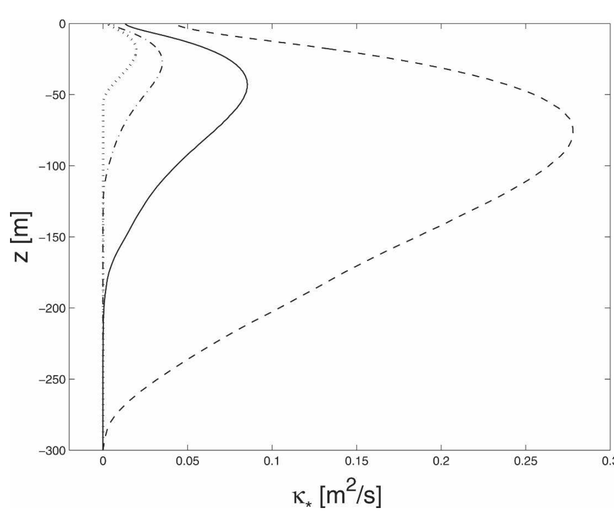

FIG. 10. Dimensional effective viscosity profiles $\kappa_*(z)$ (m^2 s^{-1}) for the same cases as Fig. 9.

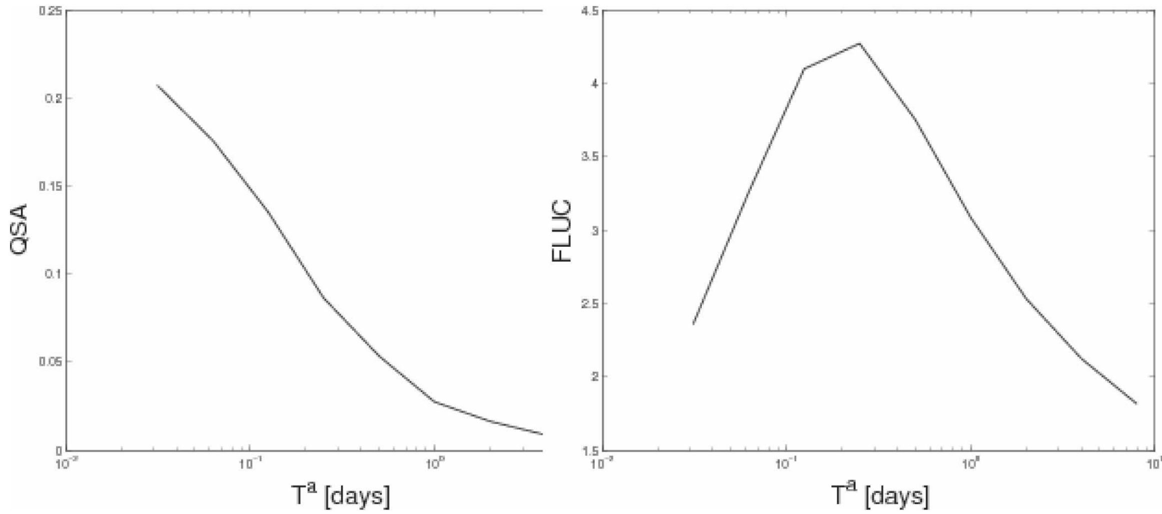

FIG. 11. (left) The normalized magnitude of the error in the mean current using the quasi-stationary approximation [i.e., QSA from (23)] and (right) the normalized magnitude of the fluctuating currents [i.e., FLUC from (24)] as functions of the Markov memory time, T^a. These measures are evaluated using the KPP model for a steady wind with $\overline{u}^a = 5$ m s^{-1} plus a two-dimensional, transient wind with $\Sigma_u^a = \Sigma_v^a = |\overline{u}^a|$.

the resulting mean currents are not very different from the Markov results. However, the frequency dependence of the currents for the periodic forcing is larger in the neighborhood of $\omega_0 = f$ due to inertial resonance (Crawford and Large 1996), with a modest minimum in RECT, a significant maximum in QSA, a very large maximum in FLUC (limited only by $R \neq 0$), and a substantial increase in β. In contrast, when $\omega_0 \approx -f$, none of these extrema occur in a pronounced way. Interestingly, in the high-frequency limit ($\omega_0/f \rightarrow \infty$), the rectification remains large (RECT $\rightarrow$ 0.87), the quasi-stationary approximation is not too erroneous (QSA $\rightarrow$ 0.24), and the current fluctuations weaken (FLUC $\sim f/\omega_0 \rightarrow 0$). On the other hand, the current and depth scaling of the Ekman layer (e.g., in the mixed layer model for elemental rectification) suggest that it has a turbulent eddy turnover time of $O(1/f)$; this indicates that a boundary layer model such as KPP should not be trusted for the current response when $\omega_0 \gg f$.

Last, we remark that the KPP model indicates very little rectification as a direct consequence of the presence of inertial currents. This is demonstrated by solving for the response to a steady wind abruptly turned on at an initial time when the current is zero. The current subsequently oscillates about its long-time mean depth profile with an inertial component whose amplitude decays at the rate R. In such a solution, the time-averaged current is virtually the same while the inertial currents are strong, as it is later after the inertial currents have decayed away. This insensitivity is because κ in the KPP model does not depend upon the changing current direction for a uniform density ocean, and after a few inertial periods the inertial currents have a depth-independent structure within the boundary layer and thus are independent of κ in their own evolution.[3] This is in contrast to the significant directional dependence when h is determined by a critical bulk Richardson number, instead of the Ekman depth criterion in (9), and the occurrence of inertial shear instability in the strongly stratified base of the boundary layer (Large et al. 1994; Large and Crawford 1995).[4]

5. Horizontal Coriolis frequency

When $f^y \neq 0$, the Ekman currents are altered depending upon the angle of the wind. We now present solutions using the generalized KPP that rescales the diffusivity, $\kappa(z.t)$, by the factor $J(\theta, \Phi)$ (section 2 and Fig. 2).

a. Steady winds

For a steady wind, κ is smallest when θ is aligned with θ_0, that is, to the northeast (NE). Weaker mixing re-

[3] The insensitivity of κ to inertial currents means that our rectification results are insensitive to the value of the inertial-radiation decay rate R.

[4] It is, of course, likely that unstratified inertial currents are unstable in reality in ways not presently represented in the KPP model, but a clear characterization of the instability behaviors is not yet established, and thus we ignore it pro tem. Since R in (2) is estimated by fits to measured inertial-current decay, it may implicitly contain effects that are more properly interpreted as due to instability rather than interiorward radiation. Insofar as $R \ll f$, then its effect on our results is slight.

quires a larger vertical shear to balance the Coriolis force in the steady Ekman layer's momentum equation (2). Larger vertical shear implies a larger velocity, albeit in a way constrained by the transport relation (1) that is independent of f^y and κ. This is indicated by the NE depth profiles in Fig. 12 (top) that show stronger mean currents with a modestly increased surface angle from the wind ($\beta = 32.5°$, rather than 31° for $f^y = 0$) and by the $\kappa(z)$ profiles in Fig. 13 (left). Oppositely, κ is largest when the wind is to the southwest (SW), and the corresponding Ekman current is weaker but again with a comparably increased surface angle. For the orthogonal wind directions, northwest (NW) and southeast (SE), κ is slightly increased by $J > 1$, and the associated mean currents are only slightly weaker than with $f^y = 0$, and the surface angles are slightly increased ($\beta = 31.5°$). Overall we see that the effect of f^y significantly alters the Ekman current profile, consistent with the previously cited studies (Coleman et al. 1990; Zikanov et al. 2003).

b. *Rectification*

When analogous comparisons are made for the standard transient wind response (section 4), we again see significant differences due to $f^y \neq 0$ [Figs. 12 (bottom) and 13 (right)]. The decrease in stress-normalized surface velocity due to rectification is evident in Fig. 12 (cf. top and bottom), and it is due to the enhancement of vertical mixing shown in section 4. However, the interplay between rectification and f^y is somewhat more subtle than a bulk mixing enhancement through the J factor in (13). For mean wind directions parallel and opposite to θ_0 (i.e., NE and SW), the symmetrically distributed wind fluctuations are symmetric in their implied J values, and the net effect of $f^y \neq 0$ again is to rescale the mixing efficiency: the mean shear is decreased for SW winds and increased for NE winds, just as in the steady-wind cases. But for mean winds in the perpendicular quadrants, symmetric wind fluctuations have an asymmetric effect in the consequent J values, with smaller Js for fluctuations on the northeastward sides of the mean direction and larger Js on the southwestward sides. The effect is to increase the shear toward the northeast for both the SE and NW cases, bending both their mean hodographs in that direction. In this regard the $f^y = 0$ and $\neq 0$ comparisons have the opposite effects for steady and fluctuating winds in the NW case. The NE and SW cases with $f^y \neq 0$ and transient wind have β values not very far from the 32° value with $f^y = 0$ (section 4), but much more extreme β values occur in the NW ($\beta = 50°$) and SE ($\beta = 15°$) transient cases with $f^y \neq 0$.

Thus, the horizontal component of the Coriolis frequency vector has a significant influence on Ekman currents by acting to augment, diminish, or skew the rectification effect.

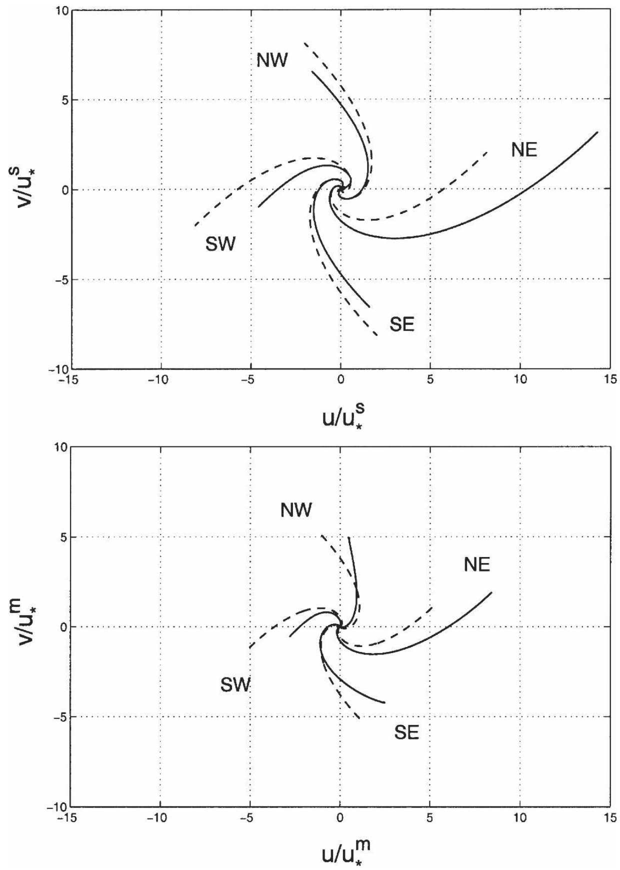

FIG. 12. Nondimensional hodographs of the mean horizontal velocity with different orientations for the mean surface stress in the labeled directions: (top) steady winds and (bottom) additional two-dimensional, transient winds with $\Sigma_u^a = \Sigma_v^a = |\overline{u}^a|$. The horizontal Coriolis frequency f^y is either zero (dashed lines) or nonzero with the value for $\Phi = \pi/6$. Normalization is by u_*, which has the values of 5.97×10^{-3} m s^{-1} (top) and 9.10×10^{-3} m s^{-1} (bottom). Parameter values are otherwise as in the standard case (e.g., Fig. 6).

6. Summary and discussion

We have shown that the unstratified Ekman layer has a significant rectification effect with transient winds: the mean current and its effective diffusivity are substantially stronger, less sheared, and deeper compared to the response to the same steady wind. While part of this rectification is due to the enhanced mean stress resulting from averaging over the quadratic (or greater) variation of stress with wind speed, $\tau \propto u_*^2 \sim |\mathbf{u}^a|^2$, a comparable part is a direct consequence of the variable

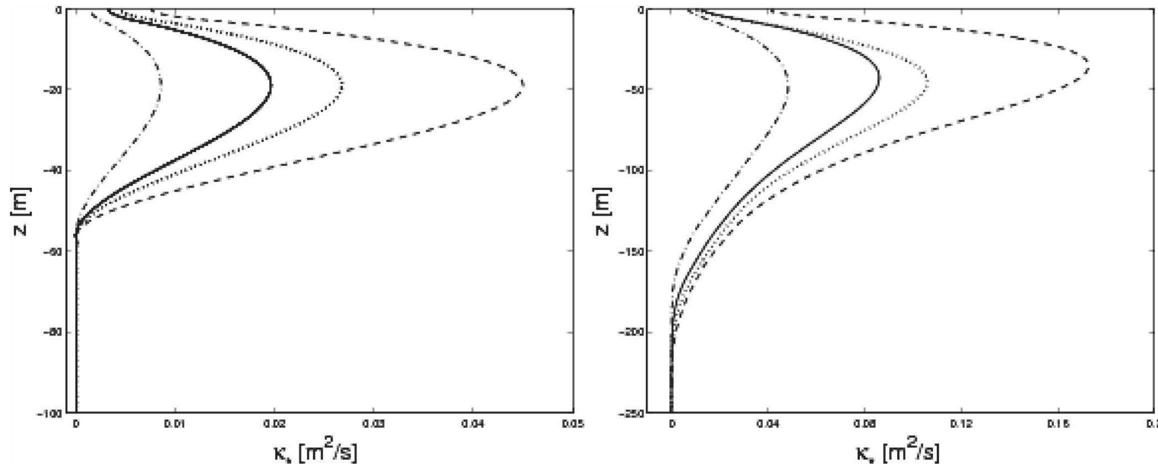

FIG. 13. Dimensional effective viscosity profiles, $\kappa_*(z)$ (m^2 s^{-1}), for the same solutions as in Fig. 12: (left) steady winds and (right) additional two-dimensional, transient winds with $\Sigma_u^a = \Sigma_v^a = |\overline{u}^a|$. In each plot, the solid line is for $f^y = 0$, and the other lines are for $f^y \neq 0$ with different mean wind directions: SW (dashed line), NW and SE (dotted line), and NE (dash–dotted line). Note the change of scale for κ_* between the panels.

mixing profile that results from the nonlinear dependence of the boundary layer eddy diffusivity on the wind stress, $\kappa \sim u_*^2/f$, multiplied by the modified mean shear to produce the parameterized vertical momentum flux by turbulent eddies. The resulting scaling is $|\overline{u}| \sim u_*$ and $\overline{h} \sim u_*/f$, with u_* a composite amplitude measure of both the mean and transient wind. Furthermore, the rectification effect is significantly modulated by the dependence of Ekman currents on the wind angle through the influence of the horizontal component of the Coriolis frequency, f^y.

The rectification effect is well approximated by the quasi-stationary approximation, $\overline{u}_{QS}(z)$, a weighted integral of the steady Ekman layer response over the probability density function for the wind, independent of the detailed wind history. This provides a practical means of incorporating rectification influences in an Ekman layer parameterization merely by including the wind PDF. How important rectification effects, due to underresolved wind variability, are in practice depends upon the context: An analysis of monthly mean Ekman currents forced by monthly mean winds would be quite erroneous; 5-day averages of surface drifter displacements using 5-day mean winds would be moderately erroneous; once-per-day coupling between atmospheric and oceanic general circulation models would be accurate in some situations but not others; and oceanic calculations with a detailed wind history obviously would not have any rectification error.

This rectification study proves the importance of rectification processes. It is not yet generally relevant to oceanic conditions because of its neglect of stratification effects, including transient buoyancy fluxes and passing mesoscale eddies. The empirical fit for near-surface, tropical Ekman currents by Ralph and Niiler (1999) suggests a dimensional scaling dependence of $|\overline{u}| \sim u_* N^{1/2} f^{-1/2}$ and $\overline{h} \sim u_*(Nf)^{-1/2}$, with N some measure of the near-surface stratification, which is also the outcome of impulsive wind deepening through a uniformly stratified layer (Pollard et al. 1973). This is clearly at odds with the unstratified scaling presented here. Similarly, Price and Sundermeyer (1999) demonstrate a significant Ekman layer rectification effect due to variable surface buoyancy fluxes and near-surface stratification. It is therefore of obvious importance to extend the present study of rectification to the stratified regime, and for this purpose supporting computational turbulence studies, particularly of the f^y influence in the stratified regime, would be very helpful.

Acknowledgments. We thank Peter Sullivan (NCAR) for performing exploratory large-eddy simulations to confirm our understanding of the influence of $f^y \neq 0$ on the Ekman layer (and hope he feels inspired to carry this investigation to completion). This research was sponsored by the National Science Foundation (NSF OCE 01-37077).

REFERENCES

Andren, A., A. R. Brown, J. Graf, P. J. Mason, C.-H. Moeng, F. T. M. Nieuwstadt, and U. Schumann, 1994: Large-eddy simulation of the neutrally stratified boundary layer: A comparison of four computer codes. *Quart. J. Roy. Meteor. Soc.,* **120,** 1457–1484.

Caldwell, D. R., C. W. van Atta, and K. N. Helland, 1972: A laboratory study of the turbulent Ekman layer. *Geophys. Fluid Dyn.,* **3,** 125–160.

Chereskin, T. K., 1995: Direct evidence for an Ekman balance in the California Current. *J. Geophys. Res.,* **100,** 18 261–18 269.

——, W. D. Wilson, H. L. Bryden, A. Field, and J. Morrison, 1997: Observations of the Ekman balance at 8°30′N in the Arabian Sea during the 1995 southwest monsoon. *Geophys. Res. Lett.,* **24,** 2541–2544.

Coleman, G. N., 1999: Similarity statistics from a direct numerical simulation of the neutrally stratified planetary boundary layer. *J. Atmos. Sci.,* **56,** 891–900.

——, J. H. Ferziger, and P. R. Spalart, 1990: A numerical study of the turbulent Ekman layer. *J. Fluid Mech.,* **213,** 313–348.

Crawford, B. B., and W. G. Large, 1996: A numerical investigation of resonant inertial response of the ocean to wind forcing. *J. Phys. Oceanogr.,* **26,** 873–891.

D'Asaro, E. A., C. C. Eriksen, M. D. Levine, P. P. Niiler, C. A. Paulson, and P. Van Meurs, 1995: Upper ocean inertial currents forced by a strong storm. Part I: Data and comparisons with linear theory. *J. Phys. Oceanogr.,* **25,** 2819–2830.

Ekman, V. W., 1905: On the influence of the earth's rotation on ocean currents. *Arch. Math. Astron. Phys.,* **2,** 1–52.

Garwood, R. W., P. C. Gallacher, and P. Müller, 1985a: Wind direction and equilibrium mixed layer depth: General theory. *J. Phys. Oceanogr.,* **15,** 1325–1331.

——, P. Müller, and P. C. Gallacher, 1985b: Wind direction and equilibrium mixed layer depth in the tropical Pacific Ocean. *J. Phys. Oceanogr.,* **15,** 1332–1338.

Germano, M., U. Piomelli, P. Moin, and W. H. Cabot, 1991: A dynamic subgrid-scale eddy viscosity model. *Phys. Fluids,* **A3,** 1760–1765.

Large, W. G., and W. B. Crawford, 1995: Observations and simulations of upper-ocean response to wind events during the Ocean Storms Experiment. *J. Phys. Oceanogr.,* **25,** 2831–2852.

——, J. C. McWilliams, and S. C. Doney, 1994: Oceanic vertical mixing: A review and a model with a non-local *K*-profile boundary layer parameterization. *Rev. Geophys.,* **32,** 363–403.

Madsen, O. S., 1977: A realistic model of the wind-induced Ekman boundary layer. *J. Phys. Oceanogr.,* **7,** 248–255.

McWilliams, J. C., P. P. Sullivan, and C.-H. Moeng, 1997: Langmuir turbulence in the ocean. *J. Fluid Mech.,* **334,** 1–30.

Niiler, P. P., N. A. Maximenko, and J. C. McWilliams, 2003: Dynamically balanced absolute sea level of the global ocean derived from near-surface velocity observations. *Geophys. Res. Lett.,* **30,** 2164, doi:10.1029/2003GL018628.

Pollard, R. T., and R. C. Millard Jr., 1970: Comparison between observed and simulated wind-generated inertial oscillations. *Deep-Sea Res.,* **17,** 813–821.

——, P. B. Rhines, and R. O. R. Y. Thompson, 1973: The deepening of the wind-mixed layer. *Geophys. Fluid Dyn.,* **3,** 381–404.

Price, J. F., and M. A. Sundermeyer, 1999: Stratified Ekman layers. *J. Geophys. Res.,* **104,** 20 467–20 494.

——, R. A. Weller, and R. R. Schudlich, 1987: Wind-driven ocean currents and Ekman transport. *Science,* **236,** 1534–1538.

Ralph, E. A., and P. P. Niiler, 1999: Wind-driven currents in the tropical Pacific. *J. Phys. Oceanogr.,* **29,** 2121–2129.

Sullivan, P. P., J. C. McWilliams, and W. K. Melville, 2004: The oceanic boundary layer driven by wave breaking with stochastic variability. I: Direct numerical simulation of neutrally-stratified shear flow. *J. Fluid Mech.,* **507,** 143–174.

Terray, E. A., M. A. Donelan, Y. C. Agrawal, W. M. Drennan, K. K. Kahma, A. J. Williams III, P. A. Hwang, and S. A. Kitaigorodskii, 1996: Estimates of kinetic energy dissipation under breaking waves. *J. Phys. Oceanogr.,* **26,** 792–807.

van Meurs, P., 1998: Interactions between near-inertial mixed-layer currents and the mesoscale: The importance of spatial variabilities in the vorticity field. *J. Phys. Oceanogr.,* **28,** 1363–1388.

Weller, R. A., 1981: Observations of the velocity response to wind forcing in the upper ocean. *J. Geophys. Res.,* **86,** 1969–1977.

——, and A. J. Plueddemann, 1996: Observations of the vertical structure of the oceanic boundary layer. *J. Geophys. Res.,* **101,** 8789–8806.

Wijffels, S., E. Firing, and H. Bryden, 1994: Direct observations of the Ekman balance at 10°N in the Pacific. *J. Phys. Oceanogr.,* **24,** 1666–1679.

Zikanov, O., D. N. Slinn, and M. R. Dhanak, 2003: Large-eddy simulations of the wind-induced turbulent Ekman layer. *J. Fluid Mech.,* **495,** 343–368.